Ceramics International 43 (2017) 5311–5318

Contents lists available at ScienceDirect

Ceramics International

journal homepage: www.elsevier.com/locate/ceramint

Synthesis and study of $Y_{0.9}Ln_{0.1}VO_4$ nanophosphors and $Y_{0.9}Ln_{0.1}VO_4$@SiO_2 luminescent nanocomposites with Ln=Eu, Dy, Er

L. Alcaraz, J. Isasi*

Departamento de Química Inorgánica I, Facultad de Ciencias Químicas, Universidad Complutense de Madrid, Ciudad Universitaria s/n, 28040 Madrid, Spain

ARTICLE INFO

Keywords:
Nanocomposites
SiO_2
Core-shell
Optical properties

ABSTRACT

$Y_{0.9}Ln_{0.1}VO_4$ nanophosphors with Ln=Eu, Dy and Er samples were prepared by hydrothermal synthesis and covered with silica (SiO_2) by the Stöber method using different reaction times. The synthesized samples were investigated by X-ray diffraction (XRD), Fourier-transform infrared (FTIR) spectroscopy, transmission electron microscopy (TEM) and photoluminescence spectroscopy (PL). XRD patterns show diffraction maxima compatible with a zircon-type structure where more intense reflexions are observed in the XRD pattern of $Y_{0.9}Er_{0.1}VO_4$ sample. FTIR spectra of $Y_{0.9}Ln_{0.1}VO_4$@SiO_2 samples reveal absorption bands which can be attributed to Si-O-Si and O-Si-O stretching bands and Si-O bending vibration. In all cases, TEM micrographs of $Y_{0.9}Ln_{0.1}VO_4$ phosphors show spherical nanoparticles. Nanoparticles agglomerates covered by a silica were found in TEM micrographs of $Y_{0.9}Ln_{0.1}VO_4$@SiO_2 samples. The thickness of the silica coating is dependent on the reaction time. PL measurements show variation of the emission intensity related to the different thickness of the silica coating.

1. Introduction

Yttrium orthovanadate (YVO_4) has been used as a host for lanthanide ions (such as Eu^{3+}, Nd^{3+}, Er^{3+}, among others) based on their high absorption coefficient in the UV range leading to strong emissions of different colors [1–4]. The phonon energy in the YVO_4 host excited under UV radiation can be efficiently transferred from the excited vanadate to the luminescent center (rare-earth cations) thereby overcoming the low absorptions of parity forbidden 4f–4f transitions [4].

Over the years, different investigations have been carried out to synthesized nanopowders of lanthanide-doped YVO_4 in order to improve the luminescence emission intensity of these oxides [5–9]. The study of these materials is motivated by their potential applications such as cathode ray tube displays and high-pressure mercury lamps [10], amplifiers for optical telecommunications [11], diode-pumped solid state lasers [12] or biological labels [13]. In the latter case, lanthanide-doped YVO_4 nanopowders could be used as a biological labelling due to their low toxicity and wide range of emission [7–9,13].

Different wet chemistry methods have been used for the synthesis of trivalent lanthanide-doped YVO_4 powders with a nanometric size such as combustion of aqueous solutions [14], co-precipitation reactions [15], hydrothermal and solvothermal methods [16–18] or colloidal routes [19]. In general, nanoparticles have surface defects that cause a reduction in the intensity of their luminescence emission. Occasionally, core-shell structures have been used to correct the problem caused by defects present on the surface of luminescent nanoparticles [20].

Lanthanide-doped luminescent nanoparticles have been covered with silica using the well-known Stöber method [21] or the reverse microemulsion method. Silica is usually used as a coating material due to its high chemical stability, optical transparency, easily controllable shell thickness, low cytotoxicity and biocompatibility [9,22]. These materials are of great interest in diagnostic analysis because of their potential to be used as luminescent probes in different biological fields such as immunoassaying, DNA sequencing and clinical diagnosing [23–27]. In fact, nanophosphors covered with silica in the range of 20–200 nm sizes can avoid renal filtration, leading to prolonged residence time in the bloodstream for better observation of diseased tissues [22].

As previously described by several authors [1,2,28], nanophosphors spherical morphology is needed to obtain high brightness and a high resolution due to its corresponding high packing densities and low light scattering. In addition, in lanthanide-doped nanomaterials both phosphors size and shape and the silica coating thickness may affect luminescence quantum efficiency, energy transfer processes [33,34] and the intensity of luminescent emission. The synthesis of

* Corresponding author.
E-mail address: isasi@ucm.es (J. Isasi).

http://dx.doi.org/10.1016/j.ceramint.2017.01.069
Received 16 December 2016; Received in revised form 4 January 2017; Accepted 13 January 2017
Available online 14 January 2017

Ln^{3+}:YVO_4@SiO_2 has been described in some references [9,29,30]. However, in some cases luminescent nanoparticles not completely covered have been obtained [31,32].

In this paper, we report the study of $Y_{0.9}Ln_{0.1}VO_4$ and $Y_{0.9}Ln_{0.1}VO_4$@SiO_2 samples. $Y_{0.9}Ln_{0.1}VO_4$ nanophosphors with Ln=Eu, Dy and Er were prepared by hydrothermal synthesis. These samples were covered with silica (SiO_2). The influence of different covered reaction time on the coating and the luminescent emission intensity of the samples was assessed.

2. Materials and methods

$Y_{0.9}Ln_{0.1}VO_4$ samples with Ln=Eu, Dy and Er were prepared by hydrothermal synthesis under acid conditions. These cores were covered with silica by the Stöber method [21]. Yttrium, europium, dysprosium and erbium nitrate ($Y(NO_3)_3{\cdot}6H_2O$, $Eu(NO_3)_3{\cdot}6H_2O$, $Dy(NO_3)_3{\cdot}xH_2O$, $Er(NO_3)_3{\cdot}6H_2O$, 99.9% Strem Chemicals) as well as ammonium vanadate (NH_4VO_3, 99% Aldrich, analytical grade) were used as starting materials. Tetraethyl orthosilicate (TEOS, Merck) was used for the samples coating.

2.1. Hydrothermal synthesis of $Y_{0.9}Ln_{0.1}VO_4$

Stoichiometric amounts of the starting materials were dissolved in 30 mL of deionized water. The resulting mixtures were stirred during 20 min and subsequently placed in a Teflon-lined stainless steel autoclave. The autoclave was heated at 433 K during 24 h and cooling down at room temperature. The obtained precipitates were collected by decantation and washed with deionized water twice. Finally, the result products were dried at 373 K during 1 h.

Due to as previously reported the crystallinity of the samples is related directly to the emission intensity [2,35] the obtained powders were heated at 873 K during 3 h in order to obtain higher crystallinity. All the synthesized powders show a light yellow color.

2.2. Synthesis of $Y_{0.9}Ln_{0.1}VO_4$@SiO_2

$Y_{0.9}Ln_{0.1}VO_4$ powders were dispersed in 50 mL of deionized water, 150 mL of ethanol and 5 mL of ammonia (32%) assisted by a sonicator for 5 min. Then, 1 mL of TEOS was added slowly under magnetic stirring. In order to analyze the effects of the covered reaction time in the samples the reaction was carried out during 6 and 18 h. The resulting white powders were separated by centrifugation and washed twice with a deionized water/ethanol solution. The synthesis process of $Y_{0.9}Ln_{0.1}VO_4$@SiO_2 samples is illustrated in the Fig. 1. Samples composition, notation and synthesis conditions are summarized in Table 1.

2.3. Characterization

The structural characterization of the synthesized samples was evaluated by X-ray diffraction (XRD) and Fourier Transform infrared (FTIR) spectroscopy. XRD patterns were collected on a Philips X Pert PRO MPD diffractometer using Cu $K_{\alpha1}$ radiation. Step scans of 0.04° (2θ) in the range 10°–70° with a counting time of 1 s for each step were employed. FTIR spectra of all samples were recorded on a Prestige-21 Fourier Transform spectrophotometer using the KBr pellet technique

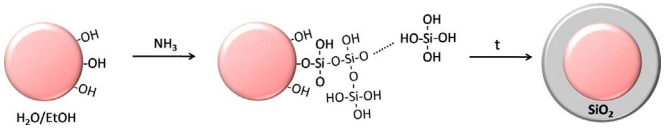

Fig. 1. Outline of the nanocomposites generation process.

Table 1
Characteristics of all cores and nanocomposites obtained.

Samples composition	Samples notation	Reaction time of the silica coating
$Y_{0.9}Eu_{0.1}VO_4$	EuC	–
$Y_{0.9}Eu_{0.1}VO_4$@SiO_2	EuS6	6 h
$Y_{0.9}Eu_{0.1}VO_4$@SiO_2	EuS18	18 h
$Y_{0.9}Dy_{0.1}VO_4$	DyC	–
$Y_{0.9}Dy_{0.1}VO_4$@SiO_2	DyS6	6 h
$Y_{0.9}Dy_{0.1}VO_4$@SiO_2	DyS18	18 h
$Y_{0.9}Er_{0.1}VO_4$	ErC	–
$Y_{0.9}Er_{0.1}VO_4$@SiO_2	ErS6	6 h
$Y_{0.9}Er_{0.1}VO_4$@SiO_2	ErS18	18 h

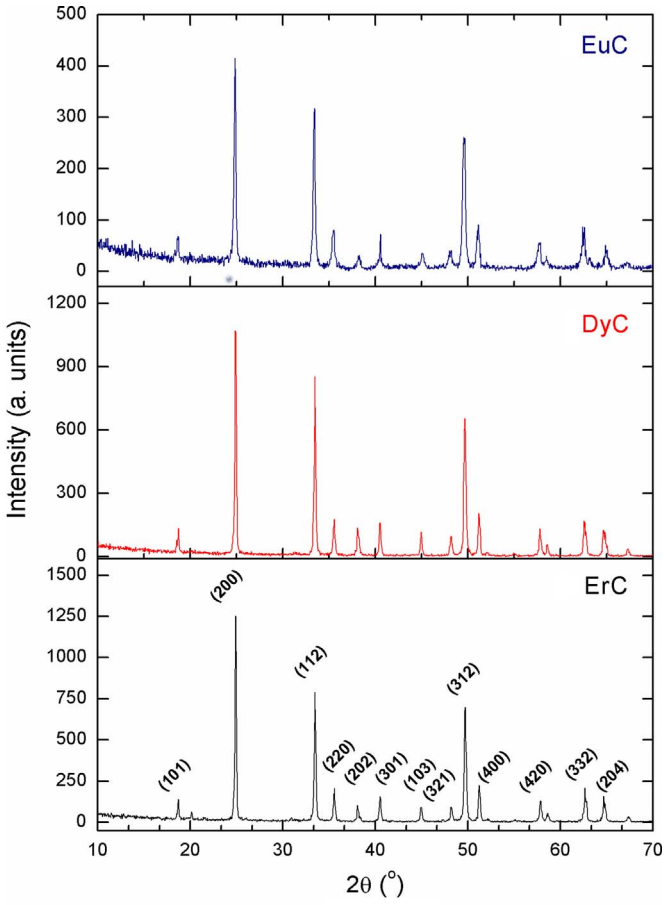

Fig. 2. XRD patterns of $Y_{0.9}Ln_{0.1}VO_4$ samples.

Table 2
Crystallographic parameters and average particle size of $Y_{0.9}Ln_{0.1}VO_4$ samples.

	a = *b* (Å)	*c* (Å)	*c*/*a*	D (nm)
EuC	7.124(5)	6.269(4)	0.88	55
DyC	7.123(7)	6.268(8)	0.88	78
ErC	7.118(2)	6.258(2)	0.88	83

within the frequency range 4000–400 cm^{-1}. The morphological characterization was carried out by transmission electron microscopy (TEM) using a JEOL JEM 2100 instrument operating at 200 kV. For TEM observations, the samples were dispersed in *n*-butanol and drops of the corresponding suspensions were deposited on carbon-coated copper

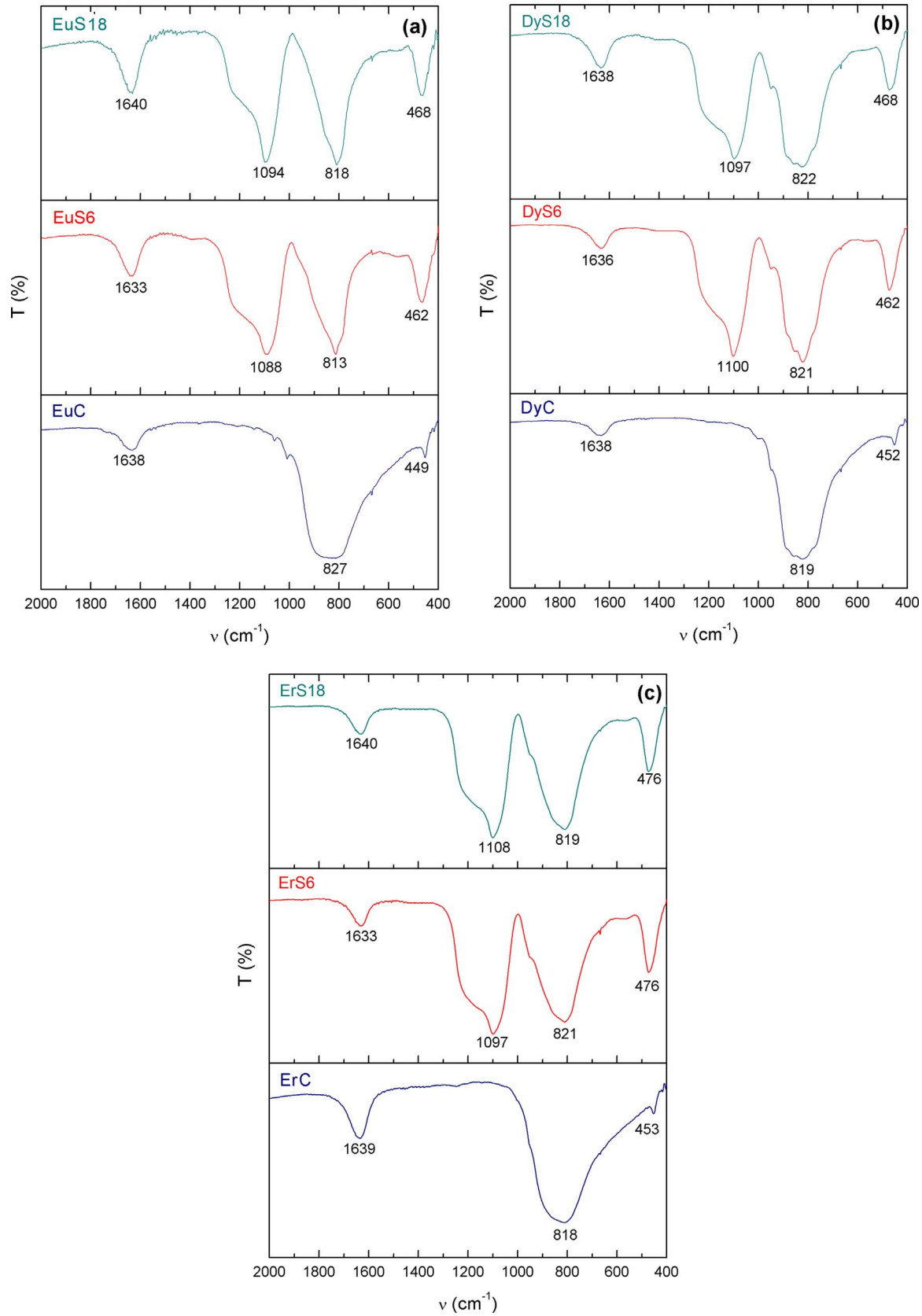

Fig. 3. Comparative FTIR spectra of $Y_{0.9}Ln_{0.1}VO_4$ and $Y_{0.9}Ln_{0.1}VO_4@SiO_2$ samples with Ln: (a) Eu^{3+}, (b) Dy^{3+} and (c) Er^{3+}.

grids. TEM-energy dispersive spectroscopy (EDS) analyses were carried out by using an OXFORD INCA instrument. Photoluminescence (PL) measurements were carried out using an excitation source, consisting in an unfocussed pulsed laser beam of about 50 femtosecond time duration at a repetition rate of 1 kHz, centered at 333 nm and 4 mW. This is produced by an optical parametric amplifier (OPA) pumped by the fundamental laser radiation from an amplified Ti: sapphire femtosecond laser system delivering 40 fs, 3.6 mJ centered at 800 nm.

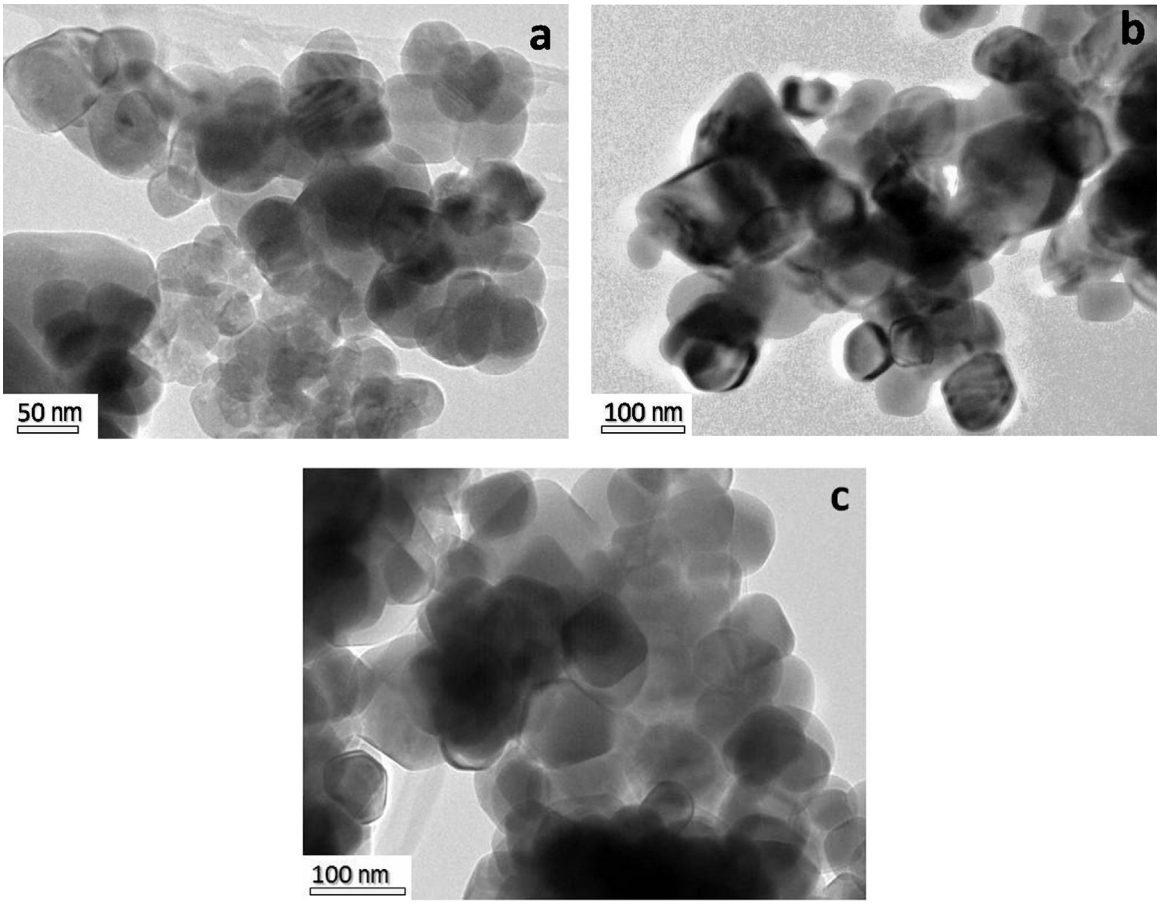

Fig. 4. TEM micrographs of samples: (a) EuC, (b) DyC and (c) ErC.

Table 3
Percentages determined by EDS microanalysis in $Y_{0.9}Ln_{0.1}VO_4$ samples.

Sample	Eu (%)	Dy (%)	Er (%)	V (%)	Y (%)
EuC	4.39	–	–	49.95	45.66
DyC	–	4.26	–	49.49	46.25
ErC	–	–	4.48	50.22	45.30
In theoretical composition (%)	5	5	5	50	45

3. Results and discussion

3.1. X-ray diffraction (XRD)

Fig. 2 shows a comparison of XRD patterns of $Y_{0.9}Ln_{0.1}VO_4$ with Ln=Eu, Dy and Er samples. All observed diffraction maxima can be indexed on the basis of a tetragonal symmetry of space group *I*41/*amd* and Z=4, compatible with a zircon-type structure [JCPDS file 00–017–0341]. No secondary peaks have been observed within the sensitivity of the experimental system used, which indicates the purity of the obtained samples. In addition, these results reveal that Ln^{3+} cations have been incorporated into YVO_4 host.

Differences in the intensity of the diffraction maxima can be observed in Fig. 2 where more intense reflections in the XRD pattern of the ErC sample while less intense maxima of EuC XRD pattern were found.

Cell parameters of $Y_{0.9}Ln_{0.1}VO_4$ samples are given in Table 2. Slightly lower lattice parameters were obtained for the ErC sample and practically similar for EuC and DyC samples. The differences obtained in the are in good agreement with the corresponding Shannon radii of Ln^{3+} cations in the environment of eight coordination in the zircon-type structure (r (Er^{3+}) =1.004 Å; r (Eu^{3+}) =1.066 Å; r (Dy^{3+})=1.027 Å) [36]. Despite of this, the c/a ratio keeps constant and equal to 0.88 in all cases.

An estimation of the average crystallite size of the $Y_{0.9}Ln_{0.1}VO_4$ synthesized samples was carried out using the Scherrer formula: $D_{hkl}=0.89\cdot\lambda/\beta_{1/2}\cdot\cos\theta$, where D_{hkl} is the crystallite size, 0.89 is the shape factor assuming spherical particles, θ is the Bragg´s angle, $\beta_{1/2}$ is the full-width at half-maximum (FWHM) of the experimental peaks (determinate from the (200), (112), (312) and (101) diffraction maxima) and λ the X-ray wavelength. The average crystallite size is also shown in Table 2. Largest particles were found for ErC sample and smaller for EuC samples in good agreement with the crystallinity observed in the XRD patterns.

3.2. FTIR spectroscopy

Comparative FTIR spectra of $Y_{0.9}Ln_{0.1}VO_4$ and $Y_{0.9}Ln_{0.1}VO_4@SiO_2$ samples are shown in Fig. 3.

Several absorption bands are observed in the 400–2000 cm^{-1} frequency range. FTIR spectra of $Y_{0.9}Ln_{0.1}VO_4$ samples show slight bands peaked at around 450 cm^{-1} which can be associated with the vibrations of Y/Ln^{3+}-O bonds [37–39]. The higher absorption bands centered around 830 cm^{-1} can be assigned to the antisymmetric stretching mode of V-O bonds present in the VO_4^{3-} units, visible in the range 780–855 cm^{-1} [40–42]. Finally, the observed band peaked at 1630 cm^{-1} can be attributed to H_2O bending vibration [43] from the adsorbed water in the KBr reagents used in the preparation of the pellets.

New absorption bands can be clearly appreciated in the FTIR spectra of $Y_{0.9}Ln_{0.1}VO_4@SiO_2$ samples which can be associated with the stretching vibration modes of the Si-O-Si (1100 cm^{-1}) and the O-

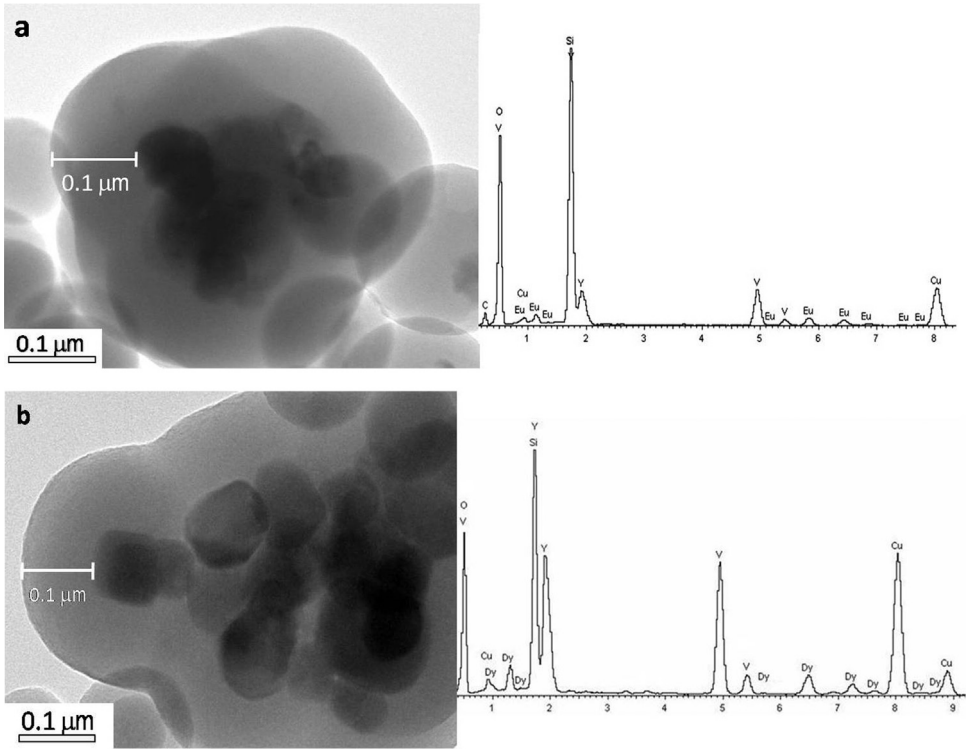

Fig. 5. TEM images (left) and EDS analysis (right) of samples: (a) EuS6, (b) DyS6 and (c) ErS6 samples.

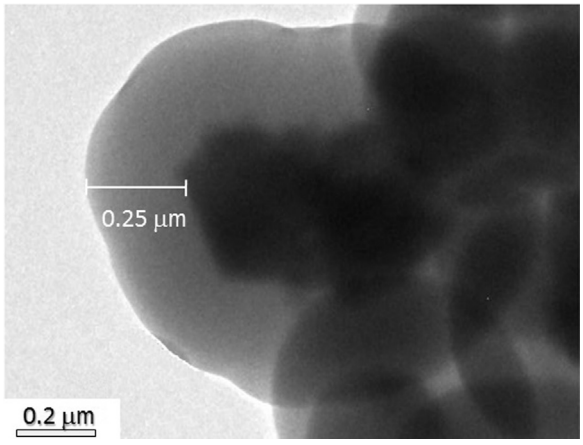

Fig. 6. TEM micrograph of ErS18 sample.

Si-O (1220 cm^{-1}) silica bonds [44,45] revealing the presence of SiO_2 in the prepared samples. In addition, an increase in the intensity of the absorption bands at 450 cm^{-1} is observed in the FTIR spectra of $Y_{0.9}Ln_{0.1}VO_4@SiO_2$ samples. This increment can be explained due to the overlap of the rocking vibration modes of the Si-O bonds which appear at 458 cm^{-1} [45,46]. Moreover, the Si-O bending vibration modes usually centered at 830 cm^{-1} [45,46] are masked in the intense bands of the spectra and they are not visible in the obtained spectra.

3.3. Transmission electron microscopy (TEM)

Fig. 4 exhibits TEM micrographs of $Y_{0.9}Ln_{0.1}VO_4$ samples. In all cases, spherical particles agglomerated can be appreciated revealing the nanocrystalline nature of the synthesized powders. Measurements carried out in up to 80 particles reveal average crystallite sizes of 50, 75 and 80 nm for EuC, DyC and ErC samples, respectively. These values are in agreement with the obtained by XRD using the Scherrer formula. EDS microanalysis carried out in different areas of the images yield atomic ratios (see Table 3) which also are in good agreement with the nominal compositions.

Fig. 5 shows TEM images of EuS6, DyS6 and ErS6 samples. The corresponding EDS analyses are also shown in Fig. 5. Particles agglomerates with a total and homogeneous covered of silica with a thickness of a 0.1 μm were found in all cases. EDS spectra confirms the presence of the different atoms in each sample. The additional signals observed of carbon (C) and copper (Cu) are due to the carbon-coated copper grids used for the measurements.

As an example, a TEM micrograph of the ErC18 sample is shown Fig. 6. Nanoparticles aggregates with a homogeneous silica coating of 0.25 μm can be appreciated. The obtained results confirm that a longer of the coating reaction time of the increases the silica covered of the synthesized samples.

3.4. Photoluminescence spectroscopy (PL)

A comparison of PL emission spectra and their enlargement of the $Y_{0.9}Ln_{0.1}VO_4$ and $Y_{0.9}Ln_{0.1}VO_4@SiO_2$ samples are shown in Fig. 7. The corresponding assignations are also included in Fig. 7. The main peaks are peaked at in the range 580–680 nm and can be attributed to the 4f–4f intraionic transitions of Eu^{3+} ion ($^5D_J \rightarrow {}^7F_J$), Dy^{3+} ion ($^4F_{9/2} \rightarrow {}^6H_{15/2}$ and $^6H_{13/2}$) and Er^{3+} ion ($^2H_{11/2}$ and $^4S_{3/2} \rightarrow {}^4I_{15/2}$) in a D_{2d} symmetry site, as expected from the substitution of Y^{3+} by Ln^{3+} in the YVO_4 host [47–55].

A significant increase of the PL emission intensity of EuS6, DyS6 and ErS6 samples can be observed. Contrary, a decrease of the emission intensity was found in PL spectra of EuS18, DyS18 and ErS18 samples. Nanomaterials with nanometric particle size exhibit high density of surface defects. These defects provide non-radiative recombination channels for electrons and holes, leading to a reduced quantum yield of the nanophosphors [56]. When luminescent nanoparticles are covered with a homogeneous silica coating lead to enhance of the luminescent emission related to structural defects or an increased surface reactivity [57,58]. On the other hand as also been reported [59,60] the decrease in the PL emission intensity of EuS18,

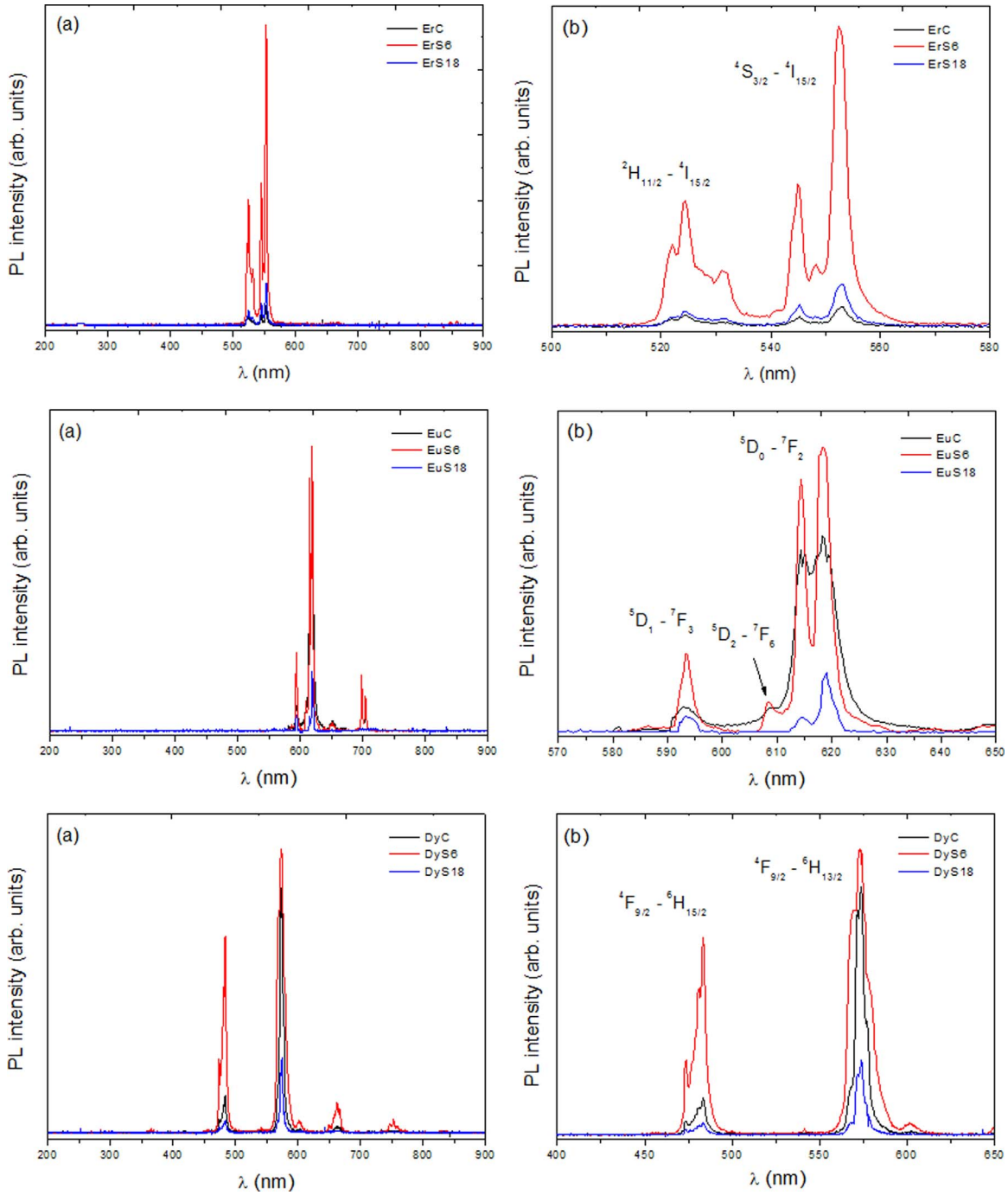

Fig. 7. Comparative (a) and elongated PL spectra (b) of $Y_{0.9}Ln_{0.1}VO_4$ cores and $Y_{0.9}Ln_{0.1}VO_4$@SiO_2 nanocomposites.

DyS18 and ErS18 samples can be explained due to the presence of silanol groups acting as luminescence quenchers. Our results illustrate that a control over the silica coating in the Ln^{3+}: YVO_4 samples can have both favorable and unfavorable effects on the PL emission intensity.

Fig. 8 shows the calculated CIE chromaticity coordinates of all samples investigated. EuC, EuS6 and EuS18 show a red emission located at (0.664, 0.327), (0.658, 0.333) and (0.599, 0.346). The yellow emission of DyC, DyS6 and DyS18 samples are located at (0.434, 0.492), (0.398, 0.449) and (0.428, 0.480), respectively. Finally, the green emission of ErC, ErS6 and ErS18 samples are located at (0.266, 0.662), (0.271, 0.702) and (0.282, 0.665), respectively.

Fig. 9 exhibits, as an example, the red bright-light of EuC, EuS6 and EuS18 powders without and under UV irradiation. In addition, Fig. 10 show the pink bright-light of a solution of EuS6 sample dispersed in water without and under UV irradiation. Quantum dots (QDs) semiconductor nanoparticles have been extensively used as luminescent labels of imaging because to its unique optical properties such as narrow emission and wide range absorption and long decay lifetimes [61,62]. However, there are considerable restrictions to the effective use of quantum dots (QDs) in bio-applications such as water dispersivity, toxicity and the stability of the QDs in biological environments [62,63]. These results exhibit that the samples investigated could be use as luminescent probes.

4. Conclusions

$Y_{0.9}Ln_{0.1}VO_4$ nanophosphors with Ln=Eu, Dy and Er were synthe-

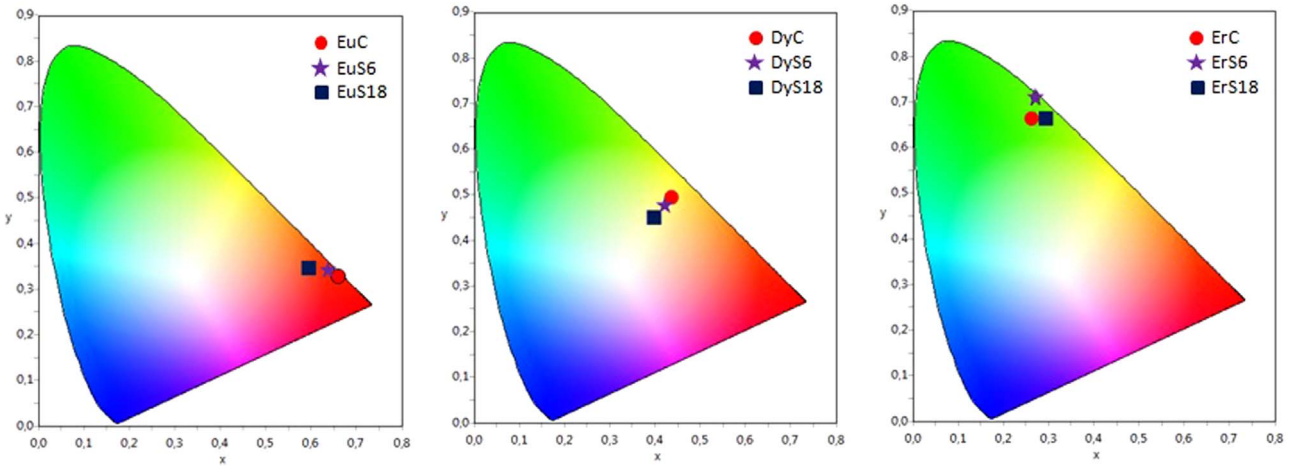

Fig. 8. The CIE chromaticity diagram of $Y_{0.9}Ln_{0.1}VO_4$ cores and $Y_{0.9}Ln_{0.1}VO_4@SiO_2$ nanocomposites with Ln^{3+}: (a) Eu^{3+}, (b) Dy^{3+} and (c) Er^{3+} excited by 333 nm laser.

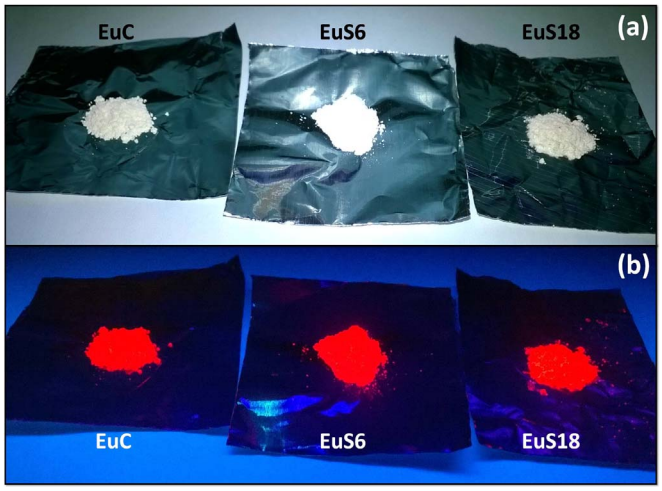

Fig. 9. EuC, EuS6 and EuS18 powder samples without (a) and under UV irradiation (b).

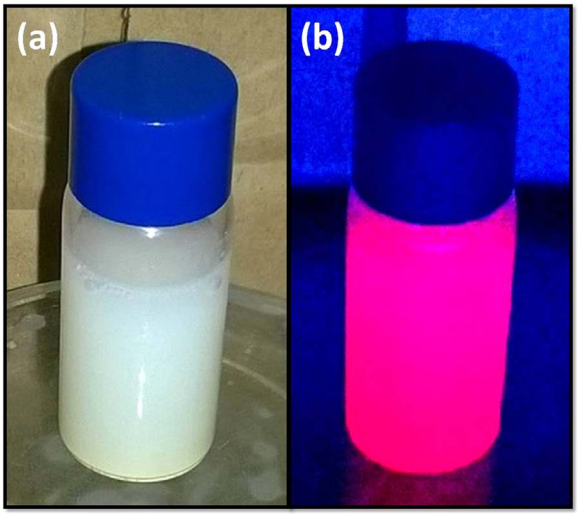

Fig. 10. Dispersed water solution of the EuS6 sample without (a) and under UV irradiation (b).

sized by hydrothermal synthesis under acid conditions. The obtained phosphors were covered with silica (SiO2) to originate $Y_{0.9}Ln_{0.1}VO_4@SiO_2$ samples. XRD patterns of the $Y_{0.9}Ln_{0.1}VO_4$ samples show diffraction maxima compatible with a zircon-type structure. $Y_{0.9}Ln_{0.1}VO_4$ FTIR spectra reveal several absorption bands assignable to Ln-O and Y-O vibration modes while FTIR spectra of $Y_{0.9}Ln_{0.1}VO_4@SiO_2$ samples show new absorption bands which can be attributed to Si-O-Si and O-Si-O stretching bands and Si-O bending vibrations. In all cases, $Y_{0.9}Ln_{0.1}VO_4$ TEM images show nanoparticles with a spherical morphology. TEM micrographs of $Y_{0.9}Ln_{0.1}VO_4@SiO_2$ samples reveal nanoparticles agglomerates with a total and homogeneous silica coating. Different coating thickness as a function of covered reaction time was found. Both $Y_{0.9}Ln_{0.1}VO_4$ and $Y_{0.9}Ln_{0.1}VO_4@SiO_2$ obtained samples exhibit strong luminescence emission. PL intensity is greater in the samples covered with a slight silica thickness as a result of a surface defects reduction. $Y_{0.9}Ln_{0.1}VO_4$ and $Y_{0.9}Ln_{0.1}VO_4@SiO_2$ synthesized samples of both powder and solution emit bright light under UV irradiation evidencing their usefulness as luminescent probes.

Acknowledgements

This work has been supported by Fundación Neurociencias y Envejecimiento through projects 177/2013 and 359/2014 and through the project BSCH-UCM GR42/15–962045.

References

[1] L. Alcaraz, J. Isasi, M. Fernández, C. Díaz-Guerra, Effect of synthesis conditions on the structural characteristics and luminescence properties of $Y_{0.9}Eu_{0.1}V_{1-x}Cr_xO_4$ ($0 \le x \le 0.5$) nanopowders, Mater. Chem. Phys. 145 (2014) 18–26.
[2] L. Alcaraz, J. Isasi, C. Diaz-Guerra, Effects of preparation method and pH variation on the structural characteristics and luminescence properties of $Y_{0.9}Er_{0.1}VO_4$ and $Y_{0.9}Er_{0.1}V_{0.9}Cr_{0.1}O_4$ nanopowders, J. Lumin. 165 (2015) 105–114.
[3] L. Alcaraz, J. Isasi, A.C. Caballero, J.G. Izquierdo, L. Bañares, Nanopowders $Y_{1-y}Nd_yV_{1-x}Cr_xO_4$ with y=0 and 1; x=0, 0.1, 0.2 and 0.5 synthesized by a sol-gel process. Relationship between morphological characteristics and optical properties, J. Lumin. 161 (2015) 110–116.
[4] R. Kim, W. Qin, G. Wei, G. Wang, L. Wang, D. Zhang, K. Zheng, N. Liu, Growth of SiO_2 hierarchical nanostructure on SiC nanowires using thermal decomposition of ethanol and titanium tetrachloride and its FTIR and PL property, Mater. Chem. Phys. 119 (2010) 309–314.
[5] J. Wang, M. Hojamberdiev, Y. Xu, Effects of different organic additives on the formation of $YVO_4:Eu^{3+}$ microspheres under hydrothermal conditions, Solid State Sci. 13 (2011) 1401–1406.
[6] B.K. Grandhe, V.R. Bandi, K. Jang, S. Ramaprabhu, S.S. Yi, J.H. Jeong, Enhanced red emission from $YVO_4:Eu^{3+}$ nanophosphors prepared by simple coprecipitation method, Electron. Mater. Lett. 7 (2011) 161–165.
[7] P. Yang, Z. Quan, Z. Hou, C. Li, X. Kang, Z. Cheng, J. Lin, A magnetic, luminescent and mesoporous core–shell structured composite material as drug carrier, Biomaterials 30 (2009) 4786–4795.
[8] H. Peng, G. Liu, X. Dong, J. Wang, J. Xu, W. Yu, Preparation and characteristics of $Fe_3O_4@YVO_4:Eu^{3+}$ bifunctional magnetic–luminescent nanocomposites, J. Alloy. Compd. 509 (2011) 6930–6934.
[9] M. Ocaña, E. Cantelar, F. Cussó, facile single-step procedure for the synthesis of luminescent Ln^{3+}:yvo4 (Ln = Eu or Er + Yb)-silica nanocomposites, Mater. Chem. Phys. 125 (2011) 224–230.
[10] R. Han, R. Hu, K. Chen, CTAB-assisted precipitation synthesis and photoluminescence properties of olive-like YVO_4:Eu nanocrystallites, Opt. Mater. 32 (2009) 329–333.

[11] R. Peretti, A.M. Jurdyc, B. Jacquier, W. Blanc, B. Dussardier, Spectroscopic signature of phosphate crystallization in erbium-doped optical fiber performs, Opt. Mater. 33 (2011) 835–838.
[12] A. Sennaroglu, Efficient continuous-wave operation of a diode-pumped Nd: yvo_4 laser at 1342 nm, Opt. Commun. 164 (1999) 191–197.
[13] G. Wang, Q. Peng, Y. Li, Lanthanide-doped nanocrystals: synthesis, optical-magnetic properties, and applications, Acc. Chem. Res. 44 (2011) 322–332.
[14] S. Ekambaram, K.C. Patil, Rapid synthesis and properties of $FeVO_4$, $AlVO_4$, YVO_4 and Eu^{3+}-doped YVO_4, J. Alloy. Compd. 217 (1995) 104–107.
[15] L. Yanhong, H. Guangyan, Synthesis and luminescence properties of nanocrystalline $YVO_4:Eu^{3+}$, J. Solid State Chem. 178 (2005) 645–649.
[16] F. He, P. Yang, N. Niu, W. Wang, S. Gai, D. Wang, J. Lin, Hydrothermal synthesis and luminescent properties of $YVO_4:Ln^{3+}$(Ln = Eu, Dy, and Sm) microspheres, J. Colloid Interf. Sci. 343 (2010) 71–78.
[17] J. Wang, M. Hojamberdiev, Y. Xu, Effects of different organic additives on the formation of $YVO_4:Eu^{3+}$ microspheres under hydrothermal conditions, Solid State Sci. 13 (2011) 1401–1406.
[18] A. Huignard, V. Buissette, G. Laurent, T. Gacoin, J.P. Boilot, Synthesis and Characterizations of YVO_4:Eu Colloids, Chem. Mater. 14 (2002) 2264–2269.
[19] A. Huignard, T. Gacoin, J.P. Boilot, Synthesis and luminescence properties of colloidal YVO_4:Eu phosphors, Chem. Mater. 12 (2000) 1090–1094.
[20] L. Tang, K. Ding, N. Chen, G. Du, An ion adsorption–diffusion process for preparing $YVO_4:Eu^{3+}@SiO_2$ core-shell nanoparticles with strong luminescence, Ceram. Int. 40 (2014) 9621–9628.
[21] W. Stöber, A. Fink, E. Bohn, Controlled growth of monodisperse silica spheres in the micron size range, J. Colloid Interface Sci. 26 (1968) 62–69.
[22] L. Liu, H. Xiao, X. An, Y. Zhang, R. Qin, L. Liu, D. Zhang, R. Sun, L. Chen, Synthesis and photoluminescence properties of core–shell structured $YVO_4:Eu^{3+}@SiO_2$ nanocomposites, Chem. Phys. Lett. 619 (2015) 169–173.
[23] J.H. Park, L. Gu, G.V. Maltzahn, E. Ruoslahti, S.N. Bhatia, Biodegradable luminescent porous silicon nanoparticles for *in vivo* applications, Nat. Mater. 8 (2009) 331–336.
[24] D.K. Yi, S.T. Selvan, S.S. Lee, G.C. Papaefthymiou, D. Kundaliya, J.Y. Ying, Silica-coated nanocomposites of magnetic nanoparticles and quantum dots, J. Am. Chem. Soc. 127 (2005) 4990–4991.
[25] G. Audram, A.P. Huguenard, In U.S. Patent, 4, 302 523, 1981.
[26] R.F. Ziolo, In U.S. Patent, 4, 474–866, 1984.
[27] N.M. Pope, R.C. Alsop, Y.-A. Chang, A.K. Sonith, Evaluation of magnetic alginate beads as a solid support for positive selection of CD34+ cells, J. Biomed. Mater. Res. 28 (1994) 449–457.
[28] H.S. Roh, Y.Ch Kang, Ch.H. Lee, H.D. Park, S.B. Park, Morphological control of Zn2SiO4:Mn phosphor particles by adding citric acid in spray pyrolysis process, Jpn. J. Appl. Phys. 42 (2003) 3429–3443.
[29] M.N. Luwang, R.S. Ningthoujam, S.K. Srivastava, R.K. Vatsa, Preparation on white light emitting $YVO_4:Ln^{3+}$ and silica-coated $YVO_4:Ln^{3+}$(Ln^{3+}=Eu^{3+}, Dy^{3+}, Tm^{3+}) nanoparticles by CTAB/*n*-butanol/hexane/water microemulsion route: energy transfer and site symmetry studies, J. Mater. Chem. 21 (2011) 5326–5337.
[30] J. Zhang, Y. Wang, Z. Xu, H. Zhang, P. Dong, L. Guo, F. Li, S. Xin, W. Zeng, Preparation and drug-delivery properties of hollow $YVO_4:Ln^{3+}$ and mesoporous $YVO_4:Ln^{3+}@nSiO_2@mSiO_2$ (Ln = Eu, Yb, Er, and Ho), J. Mater. Chem. B 1 (2013) 330–338.
[31] N.S. Singh, H. Kulkarni, L. Pradhan, D. Bahadur, A multifunctional biphasic suspension of mesoporous silica encapsulated with $YVO_4:Eu^{3+}$ and Fe_3O_4 nanoparticles: synergistic effect towards cancer therapy and imaging, Nanotechnology 24 (2013) 065101–065705.
[32] M. Darbandi, W. Hoheisel, T. Nann, Silica coated, water dispersible and photoluminescent $Y(V,P)O_4:Eu^{3+}$,Bi^{3+} nanophosphors, Nanotechnology 17 (2006) 4168–4173.
[33] H.S. Peng, H.W. Song, B.K. Chen, Temperature dependence of luminescent spectra and dynamics in nanocrystalline $Y_2O_3:Eu^{3+}$, J. Chem. Phys. 118 (2003) 3277–3282.
[34] W.O. Gordon, J.A. Carter, B.M. Tissue, Long-lifetime luminescence of lanthanide-doped gadolinium oxide nanoparticles for immunoassays, J. Lumin. 108 (2004) 339–342.
[35] L. Alcaraz, J. Isasi, C. Diaz-Guerra, M. Peiteado, A.C. Caballero, Preparation of $Ca_{0.5}Zr_2(PO_4)_3$ and $Ca_{0.45}Eu_{0.05}Zr_2(PO_4)_3$ nanopowders. Structural characterization and luminescence emission study, J. Phys. D Appl. Phys. 49 (2016) 115501.
[36] R.D. Shannon, Revised effective ionic radii and systematic studies of interatomic distances in halides and chalcogenides, Acta Cryst. A 32 (1976) 751–767.
[37] Y. Liang, J. Ouyang, H. Wang, W. Wang, P. Chui, K. Sun, Synthesis and characterization of core-shell structured $SiO_2@YVO_4:Yb^{3+}$, Er^{3+} microspheres, Appl. Surf. Sci. 258 (2012) 3689–3694.
[38] R.S. Ningthoujama, L. Robindro Singh, V. Sudarsan, S. Dorendrajit Singh, Energy transfer process and optimum emission studies in luminescence of core-shell nanoparticles: yvo_4:eu-yvo_4 and surface state analysis, J. Alloy. Compd. 484 (2009) 782–789.
[39] M. Yu, J. Lin, Z. Wang, J. Fu, S. Wang, H.J. Zhang, Y.C. Han, Fabrication, patterning, and optical properties of nanocrystalline YVO_4:a (A= Eu^{3+}, Dy^{3+}, Sm^{3+}, Er^{3+}) phosphor films via sol-gel soft lithography, Chem. Mater. 14 (2002) 2224–2231.
[40] R.L. Frost, K.L. Erickson, M.L. Weier, O. Carmody, Raman and infrared spectroscopy of selected vanadates, Spectrochim. Acta A 61 (2005) 829–834.
[41] B.K. Grandhe, V.R. Bandi, K. Jang, S. Ramaprabhu, S.S. Yi, J.H. Jeong, Enhanced red emission from $YVO_4:Eu^{3+}$ nanophosphors prepared by simple co-precipitation method, Electron. Mater. Lett. 7 (2011) 161–165.
[42] B.K. Grandhe, V.R. Bandi, K. Jang, S. Ramaprabhu, H. Lee, D. Shin, S. Yi, J. Jeong, Multiwall carbon nanotubes assisted synthesis of $YVO_4:Eu^{3+}$ nanocomposites for display device applications, Compos. Part B-Eng. 43 (2012) 1192–1195.
[43] D. Lin-Vien, N.B. Colthup, W.G. Fateley, J.G. Grasselli, The Handbook of IR and Raman Characteristic Frequencies of Organic Molecules, Academic Press, 1991.
[44] Y. Wang, W. Qin, J. Zhang, C. Cao, S. Lü, X. Ren, Photoluminescence of colloidal YVO_4:eu/sio_2 core/shell nanocrystals, Opt. Commun. 282 (2009) 1148–1153.
[45] H. Wang, M. Yu, C.K. Lin, J. Lin, Core-shell structured $SiO_2@YVO_4:Dy^{3+}/Sm^{3+}$ phosphor particles: sol-gel preparation and characterization, J. Colloid Interf. Sci. 300 (2006) 176–182.
[46] Y. Liang, J. Ouyang, H. Wang, W. Wang, P. Chui, K. Sun, Synthesis and characterization of core-shell structured $SiO_2@YVO_4:Yb^{3+}$, Er^{3+} microspheres, Appl. Surf. Sci. 258 (2012) 3689–3694.
[47] J.A. Capobianco, P. Kabro, F.S. Ermeneux, R. Moncorgé, M. Bettinelli, E. Cavalli, Optical spectroscopy, fluorescence dynamics and crystal-field analysis of Er^{3+} in YVO_4, Chem. Phys. 214 (1997) 329–340.
[48] C.A. Morrison, R.P. Leavitt, Spectroscopic properties of triply ionized lanthanides in transparent host crystals. In Handbook on the physics and chemistry of rare earths, North Holland Publishing, 1982.
[49] Z. Xu, X. Kang, C. Li, Z. Hou, C. Zhang, D. Yang, G. Li, J. Lin, Ln^{3+}(Ln=Eu, Dy, Sm and Er) Ion-Doped YVO_4 Nano/Microcrystals with multiform morphologies: hydrothermal synthesis, growing mechanism and luminescent properties, Inorg. Chem. 49 (2010) 6706–6715.
[50] K. Riwotzki, M. Haase, Colloidal YVO_4:Eu and $YP_{0.95}V_{0.05}O_4$:Eu nanoparticles: luminescence and energy transfer processes, J. Phys. Chem. B 105 (2001) 12709–12713.
[51] G. Pan, H. Song, Q. Dai, R. Qin, X. Bai, B. Dong, L. Fan, F. Wang, Microstructure and optical properties of Eu^{3+} activated $YV_{1-x}P_xO_4$ phosphors, J. Appl. Phys. 104 (2008) 084910.
[52] C. Brecher, H. Samelson, A. Lempicki, R. Riley, T. Peters, Polarized spectra and crystal-field parameters of Eu^{3+} in YVO_4, Phys. Rev. 155 (1967) 178–187.
[53] K. Riwotzki, M. Haase, Wet-chemical synthesis of doped colloidal nanoparticles: yvo_4:Ln (Ln= Eu, Sm, Dy), J. Phys. Chem. B 102 (1998) 10129.
[54] E. Cavalli, M. Bettinelli, A. Belletti, A. Speghini, Optical spectra of yttrium phosphate and yttrium vanadate single crystals activated with Dy^{3+}, J. Alloy. Compd. 341 (2002) 107–110.
[55] R. Faoro, F. Moglia, M. Tonelli, N. Magnani, E. Cavalli, Energy levels and emission parameters of the Dy^{3+} ion doped into the YPO_4 host lattice, J. Phys. Condens. Matter 21 (2009) 275501.
[56] Z. Xu, X. Kang, C. Li, Z. Hou, C. Zhang, D. Yang, G. Li, J. Lin, Ln^{3+}(Ln=Eu, Dy, Sm, and Er) non-doped YVO_4 nano/microcrystals with multiform morphologies: hydrothermal synthesis, growing mechanism and luminescent properties, Inorg. Chem. 49 (2010) 6706–6715.
[57] Y. Wang, W. Qin, J. Zhang, C. Cao, S. Lü, X. Ren, Photoluminescence of colloidal YVO_4:eu/sio_2 core/shell nanocrystals, Opt. Commun. 282 (2009) 1148–1153.
[58] P. Bo, C. Kai, G. Chao, W. Wei, The influence of SiO_2 shell on fluorescent properties of $LaF_3:Nd^{3+}/SiO_2$ core/shell nanoparticles, J. Nanomater. vol (2010) (Article ID 238792).
[59] T. Liu, W. Xu, X. Bai, H. Song, Tunable silica shell and its modification on photoluminescent properties of $Y_2O_3:Eu^{3+}@SiO_2$ nanocomposites, J. Appl. Phys. 111 (2012) 064312.
[60] M.N. Luwang, R.S. Ningthoujam, S.K. Srivastava, R.K. Vatsa, Preparation of white light emitting YVO_4: Ln^{3+} and silica-coated $YVO_4:Ln^{3+}$(Ln^{3+}=Eu^{3+}, Dy^{3+}, Tm^{3+}) nanoparticles by CTAB/*n*-butanol/hexane/water microemulsion route: energy transfer and site symmetry studies, J. Mater. Chem. 21 (2011) 5326–5337.
[61] T. Jamieson, R. Bakhshi, D. Petrova, R. Pocock, M. Imani, A.M. Seifalian, Biological applications of quantum dots, Biomaterials 28 (2007) 4717–4732.
[62] F. Mirnajafizadeh, D. Ramsey, S. McAlpine, F. Wang, P. Reece, J.A. Stride, Hydrothermal synthesis of highly luminescent blue-emitting ZnSe(*S*) quantum dots exhibiting low toxicity, Mater. Sci. Eng. C. 64 (2016) 167–172.
[63] A. Galeone, G. Vecchio, M.A. Malvindi, V. Brunetti, R. Cingolani, P.P. Pompa, In vivo assessment of CdSe-ZnS quantum dots: coating dependent bioaccumulation and genotoxicity, Nanoscale 4 (2012) 6401–6407.